ISSN 1810-2328, Journal of Engineering Thermophysics, 2011, Vol. 20, No. 4, pp. 360–379. © Pleiades Publishing, Ltd., 2011.

Radiation-Stimulated Hydrogen Transfer in Metals and Alloys

I. P. Chernov[1], **A. S. Rusetsky**[2], **D. N. Krasnov**[1*],
V. V. Larionov[1**], **T. I. Sigfusson**[1,3], and **Yu. I. Tyurin**[1***]

[1] *National Research Tomsk Polytechnic University, Tomsk, 634050 Russia*
[2] *Lebedev Physical Institute, Russian Academy of Sciences, Moscow, 119991 Russia*
[3] *Science Institute, University of Iceland, Reykjavik, Iceland*

Received June 8, 2011

DOI: 10.1134/S1810232811040059

INTRODUCTION. PROBLEM STATEMENT

Investigations of atom and molecule emission from the surface and the surface layers of solids into vacuum under different impacts have been carried out for many decades (methods and statement of some of them are reviewed in [1–9]). But only during recent 30–40 years, due to scientific and technical achievements in obtaining and diagnostics of vacuum, it has become possible to develop methods and equipment for obtaining information on the qualitative and quantitative content of various gas impurities in compact and porous solids (e.g., hydrogen, oxygen, nitrogen, water vapor, hydrocarbon gas, CO_2, CO, etc.), which are adsorbed on the surface and dissolved in the surface layer and bulk. These impurities release from heated or irradiated (by ions or electrons) materials in the form of atoms and molecules, and are detected by mass-spectrometry. In particular, it was revealed that using radiation exposure, controlling the hydrogen concentration in bulk solids, it is possible to create nonequilibrium thermodynamic systems that cannot be synthesized by traditional methods [10–12]. These problems have become urgent in recent years to researchers in different scientific areas [10, 14–16] because this allows one to achieve deep, controlled restructuring of metals and alloys on their different structure levels [10, 13].

Actively absorbing the irradiation energy, the electronic subsystem of MeH_x alloys transits to excited state. Since the frequency of collective oscillations of the hydrogen subsystem is outside the phonon spectrum of the metal crystalline lattice, its relaxation is hindered. Exposed to the electron beam in the subthreshold range, hydrogen atoms begin to actively migrate through the bulk crystal and go outside. This evidences manifestation of collective properties by the internal hydrogen metal atmosphere and is represented in a number of nonlinear effects, in particular, in the dependences of the release rate, diffusion coefficients, energy of hydrogen (deuterium) atoms on the density and energy of the exciting electron beam, or X-ray quanta. It was found that the hydrogen subsystem, preserving for a long time the supplied energy on the time scale of electronic relaxation in metals, is able to stimulate processes of rapid diffusion, nonequilibrium hydrogen escape under irradiation [11, 13].

The goal of the present work: Based on investigation of hydrogen (deuterium) release from metals under ionizing radiation in the subthreshold range, to determine the optimal conditions of dehydrogenization and consider the model of hydrogen release from metals, investigate the possibility of release of nuclear reaction products, in particular, protons and alpha particles, and also to study the mechanism of energy transfer from hydrogen to nuclear subsystem.

Contrary to the known models of electron-stimulated desorption (ESD) [1, 2], which normally use electron energies from 0.5 to several keV, in the present work we consider not only the processes of hydrogen molecule formation and detachment from metal surfaces, but also processes stimulating

---

[*] E-mail: `krasnov@tpu.ru`
[**] E-mail: `lvv@tpu.ru`
[***] E-mail: `tyurin@tpu.ru`

hydrogen diffusion from the bulk specimen, because the investigated energies amount to dozens of keV. At such energies, the depth of electron penetration into metals is several micrometers. In addition, the experiment shows that dehydrogenization at such energies occurs from the whole volume of a bulk specimen. By the bulk specimens we mean specimens whose sizes exceed by one–two orders of magnitude the sizes of electron beam cross-section. The considered model of radiation-stimulated gas release (RSG) is, probably, the first attempt to describe jointly the electron-stimulated diffusion and desorption of hydrogen (deuterium), and also nuclear reactions that accompany these processes.

Mechanisms of Hydrogen Migration under Ionizing Radiation

In metals, hydrogen can present in concentrations of $\geq 10^{19}$ cm^3 and higher, saturating split bonds, trapped by point defects, dislocations, and microcavities. Under exposure to ionizing radiation with energy under the defect formation threshold (subthreshold region), there can occur separation of hydrogen atoms from dislocation [18, 19], radiation-stimulated hydrogen desorption from grain boundaries [20], and nonequilibrium molecular hydrogen dissociation in microcavities [21]. Atomic hydrogen is extremely mobile in metals, performing to 10^{12} jumps per second (at $T = 300$ K), which is higher by 15–20 orders of magnitude than mobility of heavy impurities at the same temperatures [22]. In addition, under irradiation, the local frequencies of H-bonds lie outside the phonon spectrum of crystals, and during relaxation have to generate 3–5 phonons at once or transfer energy by the dipole (quadrupole)–charge mechanism to the electronic subsystem of solid [23]. The rate of such processes is 10^7–10^{10} s^{-1}, and before the excitation relaxation the H-bond is able to perform 10^5–10^6 oscillations. Such a state of the hydrogen subsystem provides favorable conditions for vibrational-translational exchange (V-T exchange), nonequilibrium redistribution, and hydrogen release from a solid under irradiation. For this reason, even in metals with fast relaxation in the electronic subsystem ($\tau \leq 10^{-13} \div 10^{-14}$ s), the presence of light hydrogen atoms provides conditions for temporal energy accumulation and stimulates migration of hydrogen and other impurity atoms. The electronic states of core atoms, excited by primary radiation, ensure energy transfer to the vibrational degrees of freedom of the internal H-subsystem. In these conditions, hydrogen displacement from localization sites becomes thermally nonequilibrium and is stimulated not by the energy of thermal phonons, kT, but by the long-life nonequilibrium vibrational excitations energy $\hbar\omega$ of the hydrogen subsystem. The nonequilibrium degree ($\hbar\omega/kT$) and the lifetime of the excited hydrogen subsystem in metals can be high and sufficient for stimulation of nonequilibrium diffusion and release of hydrogen and deuterium from metals under irradiation.

One more cause of the nonequilibrium hydrogen (deuterium) escape into vacuum under irradiation from a metal saturated with H and D atoms is effective lowering of the potential barrier on the way of H^+ and D^+ release from bulk metal onto the surface and their neutralization, and also acceleration of the recombination of H and D atoms into molecules and the nonequilibrium molecule desorption under electron beam exposure. A manifestation of this effect is release of all H and D atoms from the entire metal volume under irradiating only a local surface region with an area much smaller than that of the entire specimen.

1. EXPERIMENTS

1.1. The Method of Mass-Spectrometry Analysis of Desorption from Hydrogenated Metals and Investigation of Nonequilibrium Deuterium Migration through Metals. Setup for in situ Investigations

The setup is shown in Fig. 1.

Electrolythic hydrogenation was performed under the following conditions: stainless steel—1 hour, $j = 1$ A/cm^2; niobium—1 hour, $j = 100$ mA/cm^2; palladium—30 min, $j = 1$–100 mA/cm^2. The analyzed specimens in a vacuum cell were placed on a copper thermowire. The temperature was measured on the outer side of the specimen exposed to the electron beam and on the backside that was in contact with the copper substrate. It is possible to obtain reproducible experimental results on gas release by preserving identical conditions in the state of the surface. For this purpose, before electrolysis, the specimen surface was cleaned from impurities in UFH charge plasma at 40°C, a total pressure of the $H + H_2$ mixture of about 10 Pa, and plasma dissociation of $\approx 10\%$ during 20 min. Before electrolysis, the specimens were annealed in vacuum until termination of gas release, which was controlled by mass

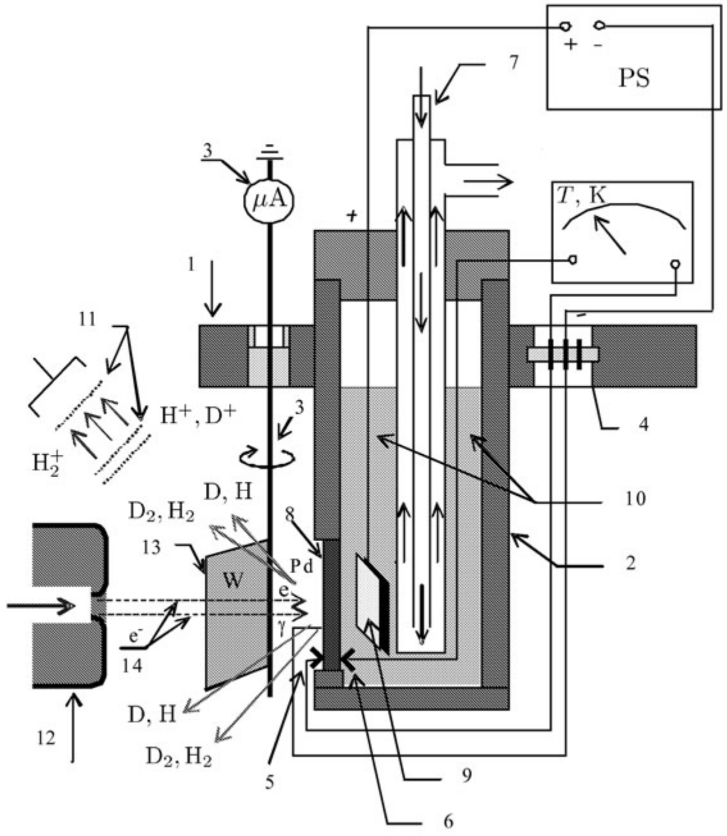

Fig. 1. A schematic cell for studying in situ processes of nonequilibrium hydrogen and deuterium migration in metals: 1—holder, 2—electrolysis cup, 3—device for measuring the electron beam current and X-ray generation, 4—vacuum current leads, 5, 6—thermocouples, 7—flow refrigerator, 8—specimen, 9—platinum electrode, 10—electrolyte, 11—mass spectrometer, 12—electron gun, 13—tungsten foil, 14—electron beam, 15—electrolyzer power supply.

spectrometry. After electrolytic hydrogenation of the specimens, their surface was again processed in low-temperature hydrogen RF discharge plasma.

The processes of stimulated deuterium release from metals were studied on specimens that were preliminary saturated during electrolysis in alkaline electrolytes: 0.1N solution of LiOD in heavy water and $H_2O + D_2O$ mixture. The setup in Fig. 1 makes it possible to combine the stage of metal saturation with hydrogen (deuterium) in the electrolytic cell and the stage of hydrogen (deuterium) release from metal under exposure to electron beam or X-ray in the vacuum chamber connected to the radiation source and the mass spectrometer. The cause was that in the case of separate saturation of the specimen in the electrolytic cell, its evacuation into atmosphere, insertion of the metal saturated with H, D atoms into the vacuum cell is inevitably accompanied by uncontrollable adsorption of particles of the gas atmosphere on the specimen and by formation of composite films on the surface of the material. Moreover, vacuum pumping of the cell with the metal specimen saturated with hydrogen (deuterium) can lead to uncontrollable evacuation of some part of injected hydrogen (deuterium) from the material under investigation. The study of the nonequilibrium hydrogen release from metals under irradiation gives in any case information on hydrogen release only from the surface and only indirectly on the hydrogen migration through the metal volume. At the same time, the fact of hydrogen penetrability of materials is of obvious interest. The mentioned problems arising in a standard method of studying the processes of nonequilibrium migration and release of hydrogen and deuterium from metals are eliminated by the cell for electrolytic saturation of metals with H and D atoms with emission of H and D atoms directly into the measurement vacuum chamber (Fig. 1). If necessary, emission of H and D atoms could be stimulated by accelerated electrons ($E = 1$–100 keV, $j_e = 1$–$150\ \mu\mathrm{A/cm}^2$) or by X-rays ($E_x = 1.0$–100 keV, $j_x = 10^{13}$–10^{15} quant/(cm^2·s)). The cell makes it possible to immediately observe electrolytic saturation of metal specimens with hydrogen (deuterium), migration of hydrogen (deuterium) through metal, and release into vacuum. A time-of-flight mass spectrometer detects the H and D atoms. As the specimens to be saturated we used Pd 0.1 mm thick; Ti, 0.05 mm thick; and Nb, 0.1 mm thick. The electron beam from the gun can be directed and focused onto the saturated specimen or can be transformed into an X-ray beam after transiting through the tungsten plate placed across the electron beam trajectory. In addition, the setup enables mass spectrometry measurements of the rate of deuterium release from metal under simultaneous action of electron beam and linear heating.

1.2. The Method of Studying the Nonequilibrium Atomic Hydrogen Release from Metals under Radiation Exposure

The mass spectrometry method, the recoil nucleus method, being highly sensitive, do not allow one to answer the questions of principal: does hydrogen emit under local irradiation from the entire specimen surface or from the site irradiated by the beam? The mentioned problems were solved by means of a method of visualizing emission of H, D atoms, using deposited dies. It is possible to observe emission of hydrogen atoms from metals under irradiation [24] using the effects of heterodyne chemiluminescence and the effect of bleaching of some kinds of organic dies deposited onto a catalytic substrate [25]. In order to prevent effects associated with X-ray and cathodoluminescent glow [1], we chose a method of visualizing the emission of H, D atoms, using appropriate dies.

1.3. The Method of Studying the Nuclear Reaction Yield under Electron and X-Ray Irradiation

In order to understand what energy can deuterium atoms accumulate under irradiation, in particular, whether it is sufficient for nuclear reactions, authors of [26, 27] investigated the yield of nuclear reaction products under exposure to 30 keV electrons for specimens of palladium and titanium saturated with deuterium. Plastic track detectors CR-39 (RadTrak) performed detection of charged particles. Two or three detectors wrapped in different-thickness foils (Al and Cu) were used to identify the type and determine the particle energy. The track detectors were preliminary calibrated by means of charged-particle accelerators and standard alpha sources. Measurement of track sizes in the detectors, using tabulated data on particle energy losses in foils, made it possible to unambiguously determine the sort of particles and their energy at the moment of escape from the specimens.

$Pd/PdO:D_x$ structures of 2.5×1 cm^2 were prepared by thermal oxidation of Pd foil (99.95% purity, 50 μm thick). As a result, an oxide PdO film ~50 nm thick was formed on the foil surface [28]. Then the specimens were saturated with deuterium in 0.3*M* solution of LiOD in D_2O with Pt anode at $j = 10$ mA/cm^2 to the saturation $x = D/Pd \sim 0.73$. The $Ti/TiO_2:D_x$ specimens of 3×1 cm^2 were fabricated from titanium foil with a 300 μm thickness and the oxide TiO_2 layer of ~ 100 nm, were

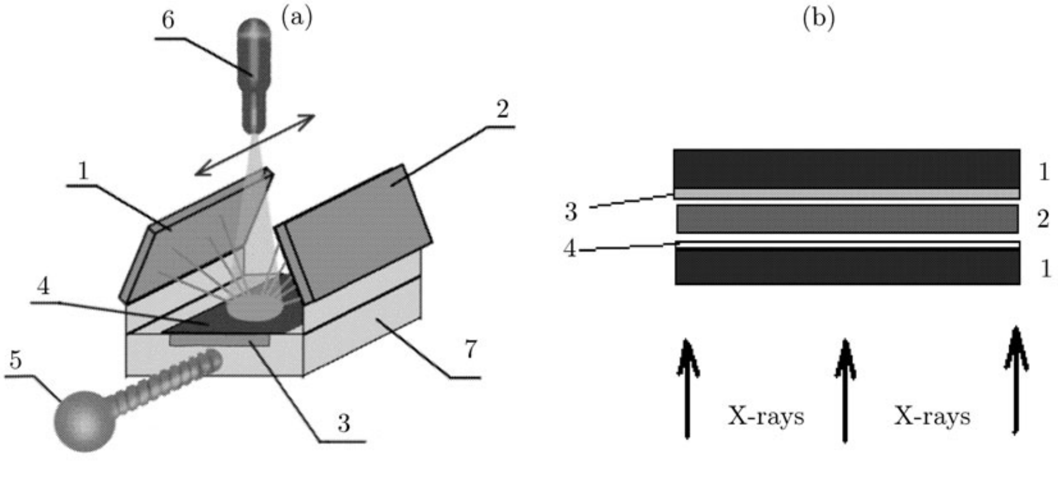

Fig. 2. Experimental scheme: (a) electron irradiation (1, 2, 3 are CR-39 detectors, 4 is specimen, 5 is manipulator, 6 is electron gun, 7 is stainless steel substrate); (b) X-ray quantum action (1 is CR-39 detectors, 2 is specimen, 3 is Cu (25 μm), 4 is Al (11 μm). The arrows show the X-ray beam direction).

saturated with deuterium from 1M solution of D_2SO_4 in D_2O at a current density of 30 mA/cm^2 during 24 hours. This provided the average saturation degree $x = D/Ti = 0.1$ to a depth of 3 μm. For investigating the effect of electrons on the yield of DD synthesis products, the specimens and detectors were placed into the vacuum chamber of the scanning electron microscope ($p = 10^{-6}$ mm Hg). The electron energy was 30 keV, the current density was 0.53–2.1 μA/cm^2, and the specimen temperature was $\sim 50°$C. Two detectors were placed above the open surface of the specimen (at an angle of 60°), detector 1 was covered with Al foil 11 μm thick; detector 2, with 25 μm Cu foil. The distance from the center of the electron spot on the specimen to the detectors was 12 mm. Detector 3 wrapped in 33 μm Al foil contacted the backside of the specimens that were not exposed to electron irradiation. In the case of investigating the effect of X-rays, the $Ti/TiO_2{:}D_x$ specimens were irradiated on an X-ray analyzer ($U = 120$ kV, $I = 5$ mA, tungsten cathode) in the air; they were placed between two detectors, 8 and 9, covered with 11 μm Al and 25 μm Cu, respectively (Fig. 2). After exposing, the detectors were etched during 7 h in 6M solution of NaOH at 70°C.

The distributions in tracks were analyzed at the P.N. Lebedev Physical Institute, RAS on the automated system PAVIKOM [29]. Only round tracks were considered (with normal incidence or with a deviation from normal of $< 10°$) for plotting the distributions. In these conditions, the total efficiency of detectors 1, 2, and detectors 3, 8, 9 was $\varepsilon = 2.6\%$ and $\varepsilon \sim 13\%$, respectively.

2. DISCUSSION OF RESULTS

2.1. Emission of Hydrogen Isotopes Stimulated by Simultaneous Radiation and Thermal Excitation

Along with the dynamics of the processes of deuterium release from metals exposed to electron beam, we carried out mass spectrometry measurements of the rate of metal deuterium release under simultaneous effect of electron beam and linear heating. The electron beam area ($d = 5$ mm, 20 mm^2 area) was much smaller than that of the specimens (200–400 mm^2) (Fig. 3). In spite of the fact that the electron beam area is much smaller than the area of the whole specimen, deuterium releases at a low temperature from the bulk specimen rather than from the region irradiated by electron beam. This behavior of hydrogen in metals can be associated with noticeable decrease of the potential barrier on the way of hydrogen release from metal into vacuum, including the processes of H^+ neutralization on the surface and H_2 stimulated desorption. Probably, there occurs effective excitation propagation

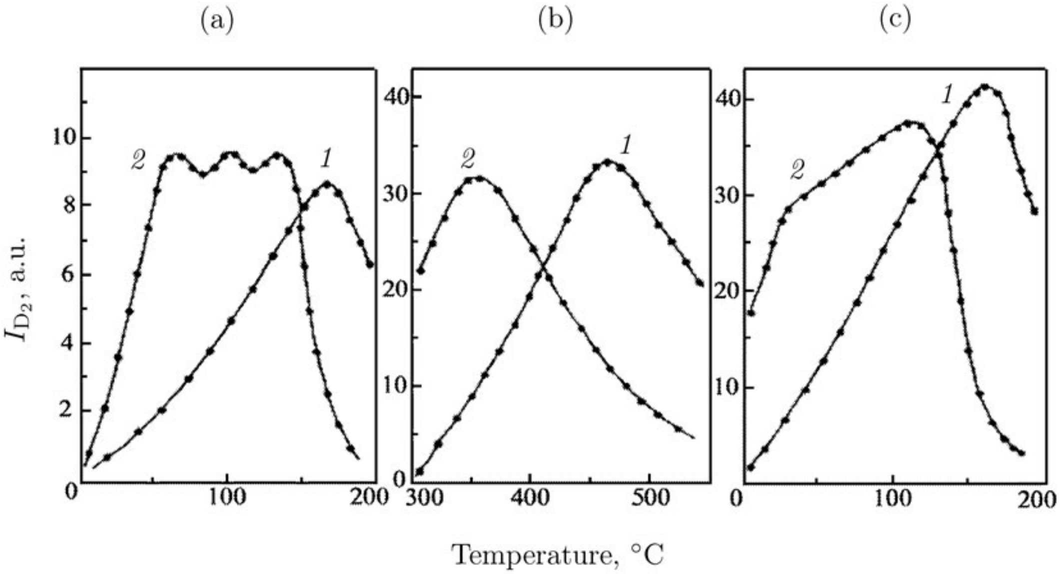

Fig. 3. Deuterium thermal release from (a) stainless steel, (b) Nb, and (c) Pd under linear heating at 0.4 K/s: 1—without electron beam; 2—with electron beam with the density (a) $j = 500$, (b) 250, and (c) 100 μA/cm^2, $E = 20$ keV.

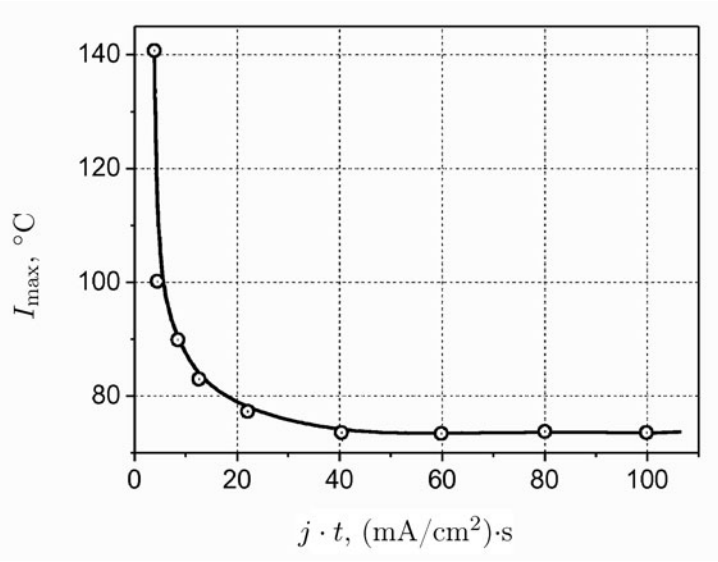

Fig. 4. The temperature maximum position on the curve of deuterium gas release from palladium under linear heating and simultaneous electron beam irradiation ($E = 20$ keV, $j = 150$ μA/cm^2) versus exposure dose of electrolytically injected deuterium, $j \cdot t$ (passed charge) (j—current density in electrolyte, t—electrolysis time).

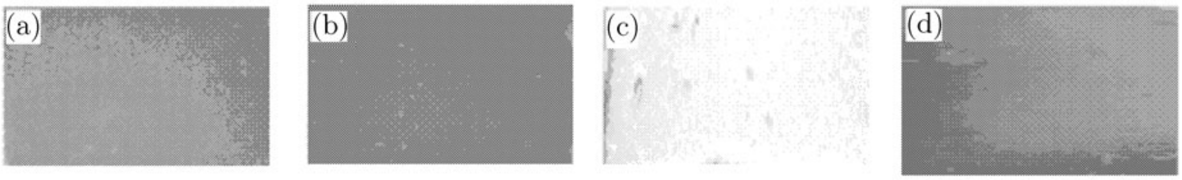

Fig. 5. A scheme of the initial experiment on die bleaching in hydrogen ($H + H_2$). Dies processed in $H + H_2$ ($D + D_2$) UHV plasma: (a) initial die; (b) processed in H_2 (D_2); (c) processed in $H + H_2$ ($D + D_2$) plasma; (d) radiation effect on the die.

in the hydrogen subsystem of metals over the whole specimen volume. This result is confirmed by nonequilibrium release of atomic hydrogen and its isotopes from metals under irradiation. The linear heating with simultaneous excitation by electron beam is accompanied in all the specimens by a shift of the position of maximum deuterium flux from palladium to a low-temperature region. The maximum gas release from stainless steel under linear heating without beam occurs at 180°C, at 80°C with the beam; from niobium—475 and 350°C, respectively; and from palladium—150 and 85°C (Fig. 4). We should note that in the Pd–D system, we observe noticeable shift of the temperature maximum of gas-release rate of deuterium under linear heating simultaneously with electron beam irradiation toward a low-temperature region as the concentration of deuterium in palladium volume is increased (Figs. 3, 4). This result also represents collective processes of excitation of the inside hydrogen metal atmosphere by electron beam.

2.2. Nonequilibrium Release of Atomic Hydrogen from Metals under Irradiation

The nonequilibrium release of atomic hydrogen from metals was investigated by means of visualization in vacuum, using deposited dies (Fig. 5).

The slowing-down radiation from the beam was attenuated by a specially designed diaphragm. The diaphragm consisted of a thin copper plate with a thick iron plate with a hole, behind it (Fig. 6). The values of mass attenuation coefficients, μ_m cm^2/g, by iron for K$_\alpha$- and K$_\beta$-lines of Cu are rather high: 302 (K$_{\alpha 1}$), 235 (K$_{\beta 1}$). The linear attenuation coefficient is $\mu = \mu_m \cdot \rho$, where $\rho = 8$ g/cm^3 is the iron density ($\mu > 1800$ cm^{-1}). For the diaphragm thickness $h = 0.4$ cm, attenuation of the primary X-ray

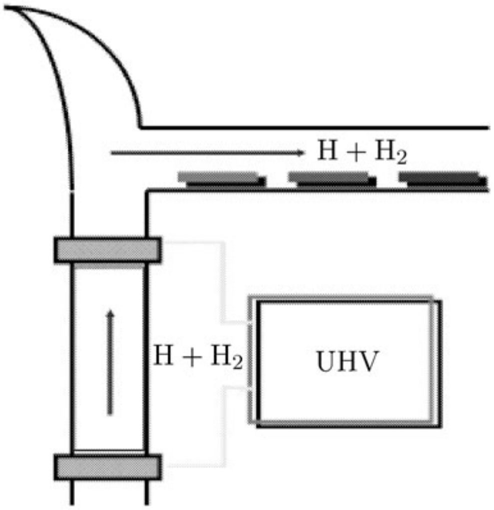

Fig. 6. A scheme of the initial experiment on die bleaching in hydrogen (Pd + D).

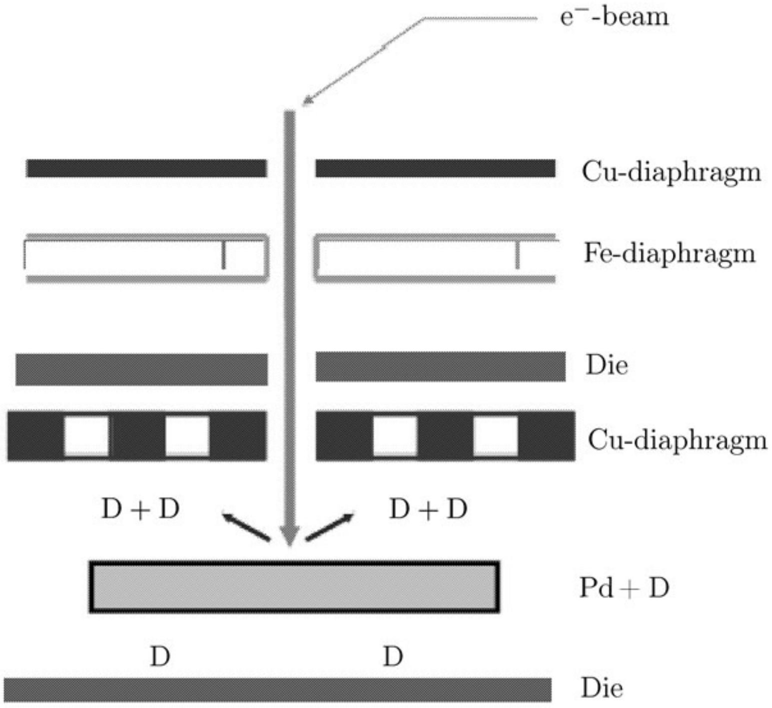

Fig. 7. A sandwich-like structure in the experiment with additional Cu-diaphragm, Pd + D, and the die.

flux is practically full. Bleaching of the dies by D and H atoms makes it possible “to see” the intensity distribution of atoms emission along the surface. This was done by means of another Cu plate with holes, which was placed between Pd and the die (Fig. 7). The sandwich was tightly compressed in order to prevent side clearances between Pd and the Cu plate with holes, the die, and the Cu plate. The performed experiment, along with the obvious result of beaching the die through the central channel, has shown that hydrogen and deuterium release proceeds with low, but quite noticeable intensity through the first channels that are nearest to the central spot, which are spaced from the central spot at 2–3 mm (Fig. 8).

We also observe weak emission of D and H atoms from the side of Pd, which is opposite to the beam

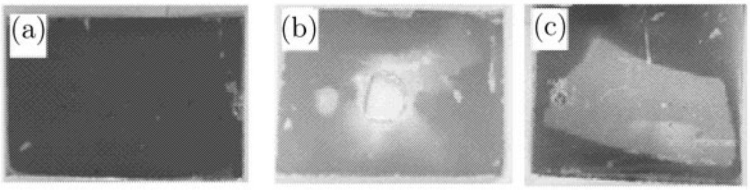

Fig. 8. Results of the experiment on atomic deuterium emission under irradiation from Pd + D to the die through the Cu-diaphragm (b) and from the not irradiated backside of Pd (c): (a) initial die; (b) upper die; (c) lower die.

effect. This is manifested in bleaching of the die in the form of Pd specimen. The die was tightly applied to the "back" unexposed side of Pd. Bleaching of the die from the opposite side is homogeneous over the entire area of its contact to Pd and has no singularities at the site exposed to the electron beam. More prominent bleaching effects are visible on the lower die along the Pd boundary. The uniform bleaching of the die from the unexposed Pd side evidences that the emission of D and H atoms does not depend on thermal heating of Pd at the site exposed to electron beam. The emission of D and H atoms from the unexposed side of Pd is associated with essential nonequilibrium in the internal D-, H-atmosphere. The temperature on the upper and lower sides of a thin ($d \sim 0.15$ mm) irradiated Pd specimen is practically the same, which was controlled by thermocouples placed on the upper and lower sides of the specimen, and did not exceed 100–150°C in our experiments.

The most important result is that the nonequilibrium deuterium (hydrogen) release from the site exposed to electron beam was experimentally proved for the first time. Of great importance is the fact that hydrogen emits from this region not only in a molecular form, but also in an atomic form. In addition, the electron beam, acting in a localized specimen region, excites the whole internal hydrogen atmosphere. An excess excitation level is sufficient also for atomic hydrogen release from neighboring metal surface regions to the site of exposure, which does not rule out more active nonequilibrium release of molecular hydrogen from the rest entire surface of the exposed metal. In addition, we also observed weak release of atomic hydrogen from the backside of a thin ($d \sim 0.15$ mm) Pd specimen under irradiation in a local area on the face side of the specimen.

Hydrogen release in an atomic form from the exposed Pd surface requires excess energy of $\approx$ 2.2 eV per hydrogen atom, compared to hydrogen release in a molecular form. Hydrogen atomization via pyrolysis requires temperatures higher than 1000 K. We knowingly did not achieve these high temperatures in our experiments, which were controlled by thermocouples placed at the site irradiated by the beam, and also by the absence of thermal luminophor quenching at the site irradiated by the electron beam. At temperatures of equilibrium hydrogen pyrolysis, the luminescence quenching would be total.

The atomic hydrogen release at rather low (200 K) Pd temperatures under electron beam exposure evidences strong disequilibrium between the hydrogen subsystem and the metal crystal lattice, and also removal of the surface potential barrier on the way of hydrogen release from the bulk metal into vacuum.

2.3. Penetrability of Metal in the System in situ: Electrolyte–Metal–Vacuum under Electron Stimulation in the Subthreshold Region

Upon placing the metal foil in the seal of a Plexiglas cup (see Fig. 1) and switching the current in the circuit Pt positive electrode Pd-window (the second electrode is negative) we do not observe instantaneous deuterium release into vacuum cell. The deuterium release becomes noticeable 1 h later for 0.05 mm Ti specimens, 30 min later for 0.1 mm Mo specimens, and 1 min later for 0.1 mm Pd specimens, at ≈ 200 mA/cm^2 electrolysis current density in $0.1N$ LiOD alkali electrolyte based on D_2O and an electrolyte temperature of 40°C. This corresponds to diffusion coefficients: $7 \cdot 10^{-9}$ cm^2/s (D–Ti), $5 \cdot 10^{-8}$ cm^2/s (D–Mo), and $2 \cdot 10^{-6}$ cm^2/s (D–Pd) at 40°C. The relative increment of the density of deuterium flux through Pd versus electron beam current density $\Delta I(\mathrm{D}, j_e)/I(\mathrm{D}, 0)$ at different electrolysis current density is given in Fig. 9. The dependence of $\Delta I/I$ on j_e is superlinear: the relative increment of the deuterium flux density reaches 100% in alkali electrolyte at 50 mA/cm^2 electrolysis current density and $j_e = 100$ μA ($E_e = 50$ keV).

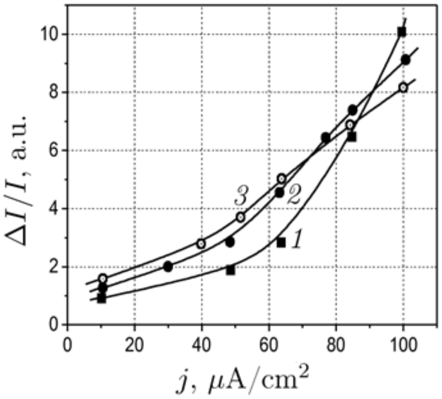

Fig. 9. The relative increment of the deuterium flux density through Pd as a function of electron beam current density ($E = 50$ keV) at different electrolysis current density: *1*—50 μA/cm^2; *2*—250 μA/cm^2; *3*—350 μA/cm^2. Alkali electrolyte.

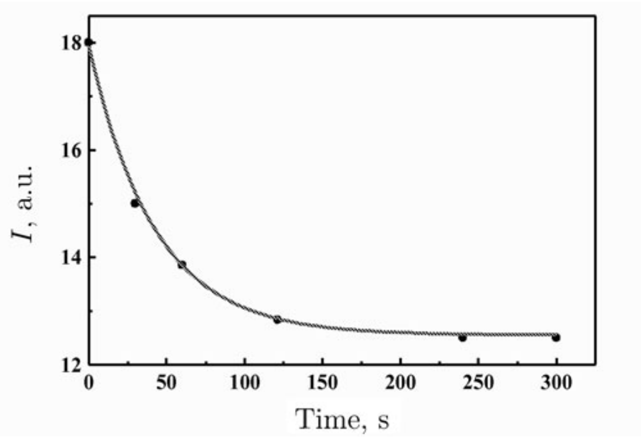

Fig. 10. Decreasing flux density through palladium at switched-off electrolysis current and switched-on electron beam ($j_e = 50$ μA/cm^2, $E = 50$ keV). Alkali electrolyte.

If we stop electrolysis, but stimulate deuterium release by electrons, the rate of deuterium release from Pd decreases slowly ($\sim t^{-1/2}$) in time (Fig. 10).

Electrolytic saturation of Pd in $0.1N$ solution of LiOD in D_2O is accompanied by forming on the Pd surface a dark film from the side of electrolyte, which contains primarily C, CH_3, CDH, CH_4, O, OH, OD, CO, COH, COD, and O_2. After 1.5–2 h work in alkali electrolyte $0.1N$ LiOD in D_2O, we observe Li emission from the vacuum side of Pd. The Li goes through Pd with a diffusion coefficient of about $D_{\mathrm{Li-Pd}} = 3 \cdot 10^{-9}$ cm^2/s. This diffusion coefficient was determined at $T \approx 330$ K and electron beam current $I \approx 60$ μA ($E = 50$ keV). The measurements on deuterium diffusion through Pd during electrolysis and the acceleration of this process under irradiation were performed also in acid electrolyte ($0.05N$ solution of H_2SO_4 in D_2O). Figure 11a represents kinetic curves of growing density of deuterium flux through palladium at different electrolysis current density. The time of attainment of saturation ranges between 2 to 6 min and decreases with decreasing electrolysis current density.

Figure 11b represents dependences of the deuterium flux density through Pd in the absence of electron current at different electrolysis current density (curve *1*) and under exposure to electron beam with a current density to 30 μA/cm^2, $E = 50$ keV (curve *2*). Curve *3* corresponds to the absolute increment of current density of deuterium release from Pd under electron beam exposure: $\Delta I = I(\mathrm{D}, j_e) - I(\mathrm{D}, 0)$ at a constant electron beam current. The absolute increment of deuterium yield depends superlinearly on the electrolysis current density.

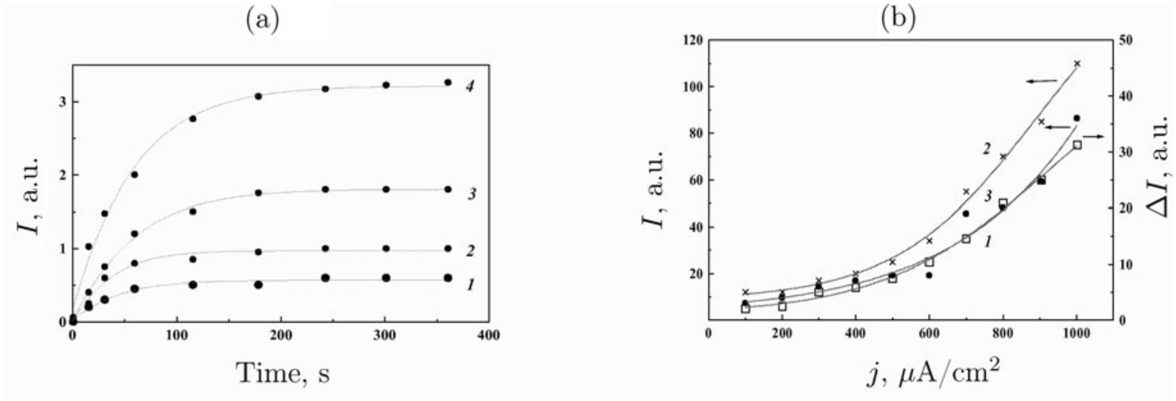

Fig. 11. Kinetic curves of growing deuterium flux density through Pd versus electrolysis current density: *1*—500, *2*—700, *3*—900, *4*—1000 μA/cm^2. Acid electrolyte. (b) Dependence of deuterium flux density I through Pd on the electrolysis current density without electron stimulation (1) and with electron stimulation ($j_e = 30$ μA/cm^2, $E = 50$ keV) (2), absolute increment of deuterium flux density through Pd with switched-on electron beam (3). Acid electrolyte.

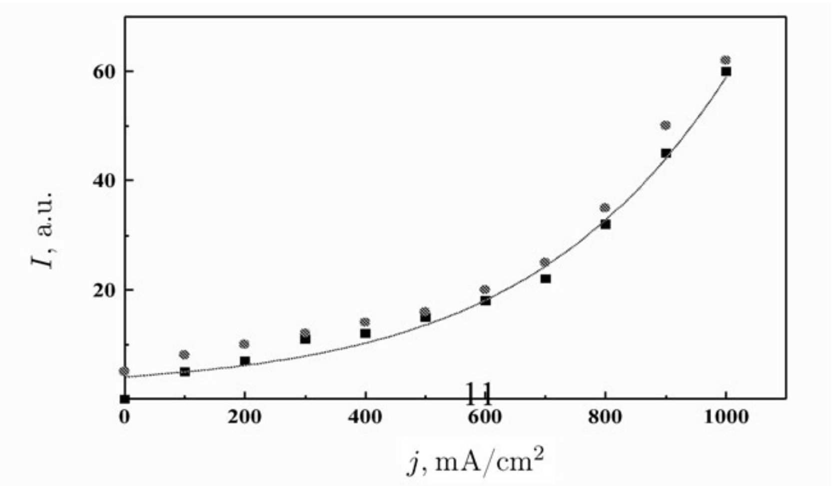

Fig. 12. Relative increment of the flux density of released deuterium from Pd for different electron beam current density and two values of electrolysis current density: (●) 500, (■) 800 μA/cm^2. Acid electrolyte.

Figure 12 represents relative increments of the flux density of released deuterium at different electron beam current density ($0 \leq j_e \leq 60$ μA/cm^2) and two values of electrolysis current density, 500 and 800 mA/cm^2. The relative increment superlinearly grows from the level of electron excitation and does not depend on the electrolysis current. The temperature of the electrolyte and the Pd membrane is kept constant. If we decrease the electrolysis current to zero, then the dependence of flux density of released deuterium on the electron beam current becomes linear (Fig. 13a). If after performing electrolytic Pd saturation with deuterium we transit to a zero electrolysis current and switch on the electron beam ($I = 60$ μA, $E = 50$ keV), then the intensity of deuterium lines linearly drops with time, at $t > 30$ min, the D line practically disappears, continuing asymptotic approach to zero (Fig. 13b).

We should note that in acid electrolyte, the absolute deuterium yield from Pd is approximately three times higher than in alkali electrolyte. The relative velocity increment of the rate of deuterium release from Pd under exposure to electron beam, $j_e = 40$ μA in acid electrolyte, is two times higher than in alkali electrolyte (approximately 60 and 30%). This result also characterizes manifestation of collective effects in the internal hydrogen atmosphere under excitation. The obtained results on deuterium and hydrogen diffusion in metals under excitation in situ evidence that there is no oversaturation and accumulation of great amount of hydrogen and deuterium in the bulk metal. Accumulation and release of hydrogen (deuterium) under irradiation from the surface contacting the electrolyte are much higher than from

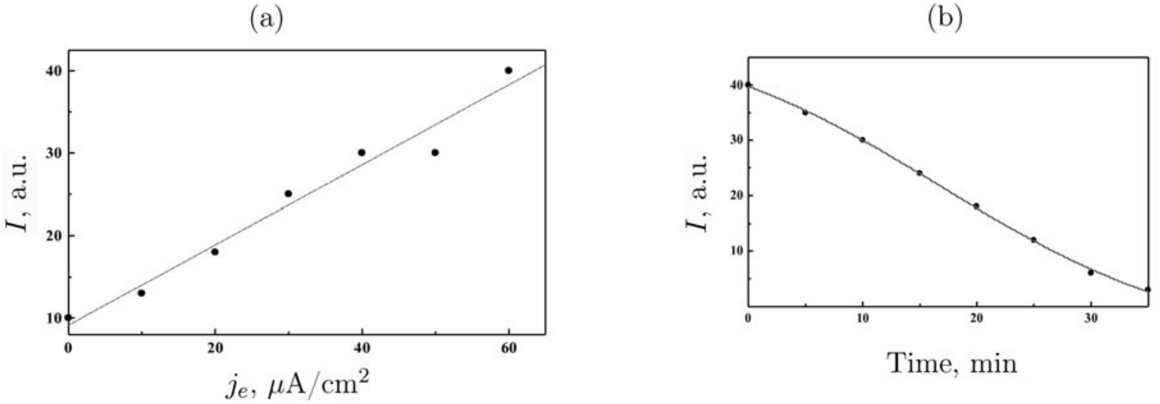

Fig. 13. (a) Dependence of the deuterium flux density from Pd at zero electrolysis current and electron-beam-stimulated deuterium emission ($j_e = 60\ \mu\text{A/cm}^2$, $E = 50$ keV). Acid electrolyte. (b) Decreasing deuterium flux density from Pd under switched-off electrolysis current and electron-beam-stimulated deuterium emission ($j_e = 60\ \mu\text{A/cm}^2$, $E = 50$ keV). Acid electrolyte.

the surface that was not saturated with hydrogen and deuterium during electrolysis, that is, the surface coming to vacuum. This result can be explained by high mobility of hydrogen and deuterium (protons and deuterons) in the bulk metal and by existence of special heterostructures in the surface region that was in contact with electrolyte. The heterostructures are microbubble and polylayer formations developing when the metal and electrolyte are in contact during electrolysis.

The developed measurement cell has made it possible to propose a new reliable and simple method for studying the hydrogen penetrability of materials and for measuring the coefficients of hydrogen and deuterium diffusion through metals for other elements, as well. At that, diffusion of these elements can be stimulated both by radiation and by nonequilibrium hydrogen atmosphere. In particular, we have shown that the coefficient of deuterium diffusion through Pd substantially grows under the action of electron beam (see Fig. 12). The new system validated the hypothesis on nonequilibrium excitation of the internal hydrogen atmosphere of metals under irradiation. It has been experimentally shown that there is practically instantaneously increasing release of deuterium from metals after activation of electron beam in the conditions of thermostatted membrane from Pd and other metals.

2.4. Emission of Positive Ions Irradiated by Palladium Electrons Saturated with Hydrogen and Deuterium

Irradiation by electrons of metals saturated with hydrogen (deuterium) stimulates nonequilibrium emission not only of H_2, DH, and D_2 molecules [10, 15] from Pd(D, H), Nb(D, H), but also free H, D atoms [16]. Since even thermally equilibrium heating of metals with an adsorption layer is accompanied by emission of positive ions [16], it is natural to expect that the radiation energy supply to metals saturated with hydrogen (deuterium) will lead to excitation of the internal hydrogen atmosphere and can stimulate nonequilibrium emission of positive ions from the metal surface. The hypothesis is experimentally validated. For this purpose, a cell with a positive ion detection sensor was added to the setup (Fig. 1). The main element of the sensor (Fig. 14) is the irradiated palladium cathode ($S = 1$ cm^2), which was electrolytically saturated with hydrogen and deuterium (0.1N LiOD alkali solution in 95% D_2O + 5% H_2O) during 15 min, $j = 1$ A/cm^2. A collecting metal anode ($S = 1$ cm^2) was nearby the cathode ($d < 8$ mm). Ejecting (for positive ions from the cathode) potential difference from 0 to 600 V was created between the cathode and anode. To prevent the effect of spurious electron currents in the system due to scattered and secondary electrons, we used locking grids ($S = 2$–3 cm^2). The grids are under negative potential relative to the cathode and anode (0–10^3 V). The distance between the grids and the cathode (anode) is under 1 mm. A moving-coil galvanometer G, 1 nA sensitivity, measured the current in the cathode-anode circuit.

The electron beam current could be varied from 1 to 100 μA, the beam energy from 0.1 to 100 keV. To prevent local heating of Pd under irradiation, the beam was defocused to a spot 5–7 mm in diameter. The temperature at the site of electron beam irradiation was controlled by thermocouples from the exposed

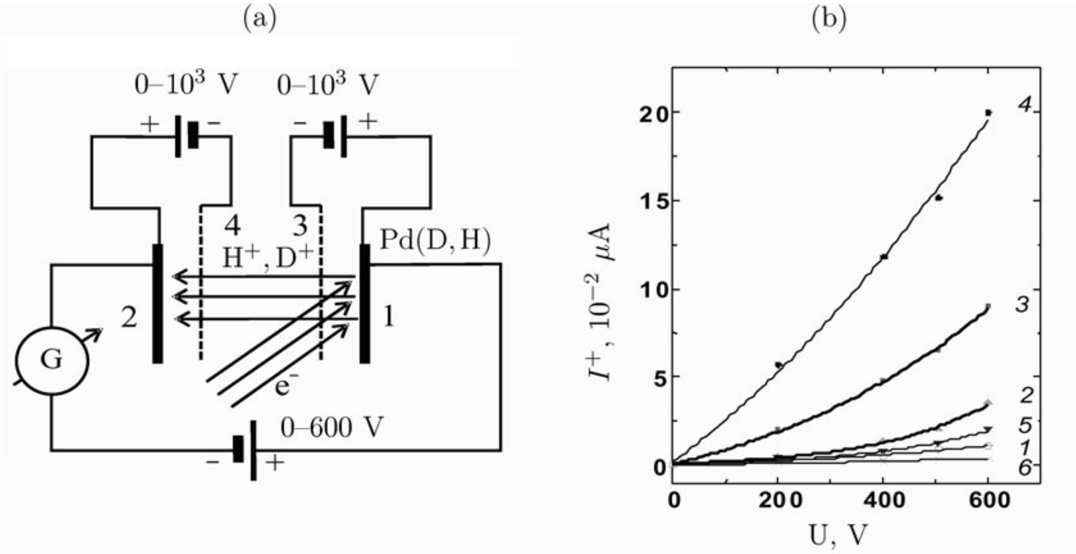

Fig. 14. (a) A circuit of the cell for detection of electron-stimulated positive ion emission from Pd(D, H): *1*—irradiated Pd(D, H) "cathode"; *2*—collecting (protons) anode; *3*, *4*—gating (electrons) grids. (b) Current-voltage characteristics of ion Pd(D, H) emitter irradiated by electrons. Electron beam currents: *1*—2 μA; *2*—4 μA; *3*—6 μA; *4*—9 μA; *5*—4 μA (irradiation with lower D and H concentration in Pd, compared to (2)); 6—X-raying of Pd(D, H).

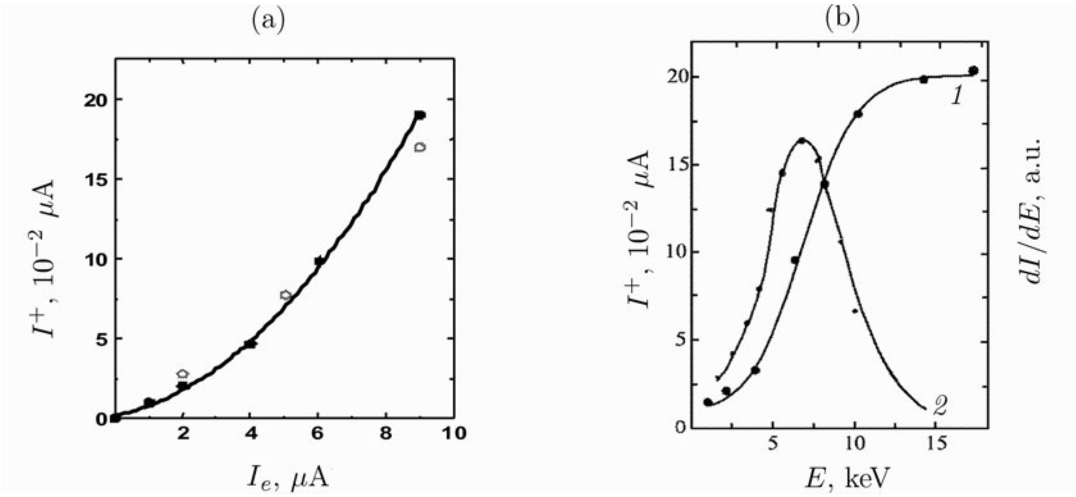

Fig. 15. (a) Positive ion emission current I^+ from Pd(D, H) versus electron beam I_e (dots—experiment; solid curve—approximation $I^+ = aI_e^2$, where $a = 2.7 \cdot 10^{-3}\ \mu\mathrm{A}^{-1}$); (b) positive ion current versus accelerated electron energy (1) and emission current distribution in electron beam energy (2). The power supplied by electron beam to Pd(D, H) ($I_eE = 0.3$ W) is constant.

and unexposed sides of Pd and was not higher than 40°C. At this temperature, the equilibrium hydrogen and deuterium yield from Pd is insignificant, and there is no emission of positive ions [16, 31].

The mechanism of nonequilibrium release of hydrogen and its isotopes from metals is associated with special accumulating properties of hydrogen in metals. If we take into account that the degree of Pd hydrogenation is high and corresponds approximately to one H(D) atom per Pd atom, the energy of plasma oscillations of the hydrogen Pd subsystem is

$$\hbar\omega = \hbar e\sqrt{\frac{\rho_{\mathrm{Pd}}N_A}{M_{\mathrm{Pd}}m_p\varepsilon_0}} \cong 0.2\ \mathrm{eV},$$

where ρ_{Pd} and M_{Pd} are the density and molar mass of palladium, m_p is the proton mass, N_A is the Avogadro number, ε_0 is the electric constant, and e is the elementary charge.

A close value of the nonequilibrium oscillation energy can be obtained from comparing the effective and the equilibrium coefficients of hydrogen diffusion to Pd.

The nonequilibrium processes of H_2, D_2 molecules, H, D atoms, and H^+, D^+ ions emission are characterized by excess of the corresponding flux densities of atoms, molecules, and current densities of ions under irradiation over thermally equilibrium values of the corresponding quantities without Pd irradiation. The specimen in the experiments was thermostatically controlled (40°C). A considerable nonequilibrium degree in the hydrogen (deuterium) Pa subsystem ($\hbar\omega/kT \cong 10$ at 313 K) can cause not only release of free atoms from the Pd surface under electron irradiation, but also emission of positive ions (H^+, D^+) [31].

Irradiating the Pd by an electron beam with a 50 keV energy and the current $I_e = 2$–10 μA, we observed emission of positive ions with a maximum current of 0.2 μA at a beam current of 10 μA (0.1, 0.04, and 0.012 at 6, 4, and 2 μA, respectively (Fig. 15a)). The current of positive ion emission drops as the hydrogen (deuterium) releases from Pd (Fig. 15b, curves *4*, *5*). Curves *2*, *5* in the figure were taken with an interval corresponding to a charge of ~ 10 C ($\sim 6 \cdot 10^{16}$ electrons, $\Delta t = 10^4$ s) through the cathode. Growing emission current of positive ions correlates with increasing hydrogen and deuterium intensity lines in mass spectra.

There is no positive ion emission under irradiation by electrons of Pd (D, H). Appearance of the positive ion current is not connected with ionization by hydrogen and deuterium electrons in the gas phase. In blank tests, irradiation by electrons of palladium not saturated with hydrogen and deuterium, with hydrogen and deuterium in the residual gas atmosphere, does not cause detectable emission current. The emission current drops nearly to zero at zero extraction voltage, which evidences low energy of nonequilibrium emission of positive ions. A low emission current of positive ions is also observed under irradiation of Pd (D, H) by γ-quanta emitted as the electron beam is decelerated by a 50 μA current in a thin tungsten layer (W, $d = 0.15$ mm). The spacing between W and Pd (D, H) decelerating the electrons did not exceed 5 mm. A peculiar feature of the obtained results is quadratic growth of positive ion emission current versus electron beam current. A good approximation of this dependence is formula (I^+ and I_e in μA): $I^+ = 2.7 \cdot 10^{-3} I_e^2$. The nonlinear growth of positive ion emission current versus the electron beam is characteristic for processes with participation of excited hydrogen atmosphere of metals. The excited hydrogen atmosphere in metal leads to growth of both the number of H, D atoms released from the bulk metal to the surface and the number of positive ions removed from the surface. A combination of these factors leads to nonlinearly growing emission current of positive ions versus electron beam current.

The dependence of the positive ion current on the accelerated electron energy and also the ion distribution as a function of electron beam energy are shown in Fig. 18. The decrease of the positive ion current with decreasing energy of accelerated electrons in the range of about 6 keV is not associated with decreasing power supplied to Pd (D, H) by the electron beam. In the experiment, the supplied power $I_e E = 0.3$ W was maintained constant—as the electron beam energy decreased, the beam current was increased.

2.5. Radiation-Stimulated Nuclear Processes in Palladium–Deuterium, Titanium–Deuterium Systems

The present paper presents results of five sessions of measuring the yield of DD-synthesis products under irradiation by $Pd/PdO{:}D_x$ electrons. In four sessions, the average electron beam density was $\sim$ 0.53 μA/cm^2 and the exposure time was $\sim$ 1100 min in one session. Repeatability of the results is good; the integral proton yields in each session are in good agreement. With regard to detection efficiency, the rate of 3 MeV proton emission from the specimen side irradiated by electrons, averaged over the data from detectors 1 and 2, was $\mathrm{Np} = (1.1 \pm 0.1) \times 10^{-3}$ R/s×cm^2, and $\mathrm{Np} = (7.2 \pm 1.6) \times 10^{-4}$ R/s×cm^2 from the opposite side, which is 1.5 times less than that for the irradiated side. In the fifth measurement session, the electron flux density was increased 4 times, to 2.1 μA/cm^2; the rate of 3 MeV proton emission averaged over detectors 1 and 2 increased two times. The emission of 3 MeV protons from the backside of the specimen shows that the deuterium atoms, during electron beam

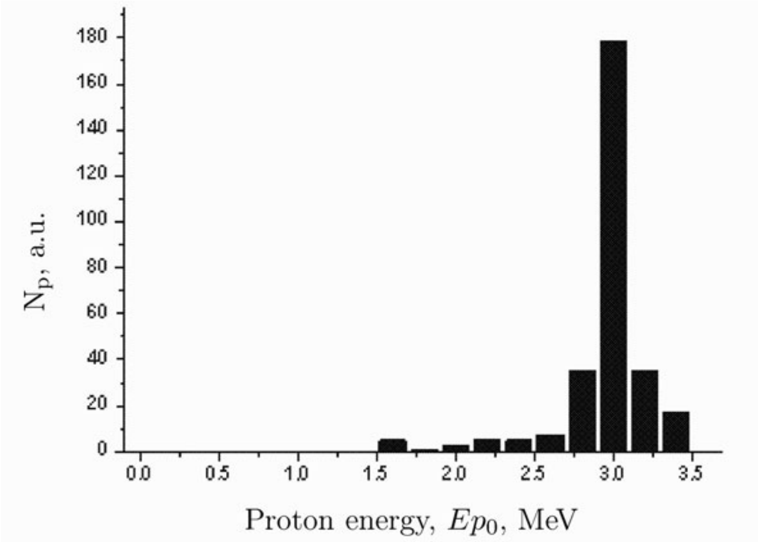

Fig. 16. The reconstructed energy spectrum of protons detected in detectors 1, 2, and 3 during $Pd/PdO{:}D_x$ irradiation by electrons with 30 keV energy and 0.53 μA current density during 7020 min.

irradiation, receive energy not only in the region of direct beam radiation, but also in the whole specimen volume. This fact confirms that the deuterium (hydrogen) subsystem in metals is excited by ionizing radiation over the whole specimen volume. Analysis of the tracks in the background detector, which was placed in the microscope vacuum chamber far from the specimens during the experiment, has shown that the spectrum does not have significant maxima in the range of track diameters from 4 to 6 μm, which correspond to nuclear synthesis products. The same result took place during long-term electron irradiation of hydrated $Pd/PdO{:}H_x$ and $Ti/TiO_2{:}H_x$ specimens.

Figure 16 illustrates a reconstructed energy spectrum of protons released by a $Pd/PdO{:}D_x$ specimen under irradiation by electrons during 7020 min and recorded by detectors 1, 2, and 3. The emission of 3 MeV protons is statistically reliably observed in three independent detectors, which unambiguously evidences DD-synthesis in the $Pd/PdO{:}D_x$ specimens under irradiation by electron beam.

Analysis of track diameters in detectors 1 and 2 after irradiation of the $Ti/TiO_2{:}D_x$ specimen by electrons with a 30 keV energy and 0.53 μA current density during 2200 min, and in detectors 8 and 9 that were in contact with the $Ti/TiO_2{:}D_x$ specimen under X-raying ($I = 100$ mA, $U = 120$ kV, and irradiation time 240 min) has shown that in the distributions the main peak is observed in the range of 5.0–6.6 μm, which shifts to the right with growing thickness of the coating. According to the calibration data, the peak is identified as a signal from 3 MeV protons. Thus, the action of accelerated electrons and X-rays on the $Ti/TiO_2{:}D_x$ stimulates release of 3 MeV protons, as in the case of the action of electrons on the $Pd/PdO{:}D_x$ specimens.

The reconstructed energy spectra of protons and alpha particles, which are emitted by the $Pd/PdO{:}D_x$ specimens during irradiation by the electron beam and detected by detectors 1, 2, and 3, are represented in Figs. 17a and 17b. It is seen that emission of 11–17 MeV alpha particles and 3 MeV protons is statistically reliably observed in three independent detectors, which evidences DD-reactions in the $Pd/PdO{:}D_x$ specimens under exposure to electron beam. It is noteworthy that under the action of electron beam on the $Pd/PdO{:}D_x$ and $Ti/TiO_2{:}D_x$ specimens, the energy of the emitted protons is 3 MeV from both irradiated and not irradiated sides of the specimen. Therefore, the nuclear processes run primarily in the near-surface region of the specimen, probably, at the Pd–PdO, $Ti–TiO_2$ interface. This situation may be caused by a higher deuterium concentration at the metal–dielectric interface because the radiation-stimulated deuterium diffusion in metals is much higher than in metal oxides. Table 1 represents proton yields stimulated by electron and X-ray beams on $Pd/PdO{:}D_x$ and $Ti/TiO_2{:}D_x$. The table shows that the yields of 3 MeV protons from the $Pd/PdO{:}D_x$ and $Ti/TiO_2{:}D_x$ specimens stimulated by 30 keV electrons are nearly the same.

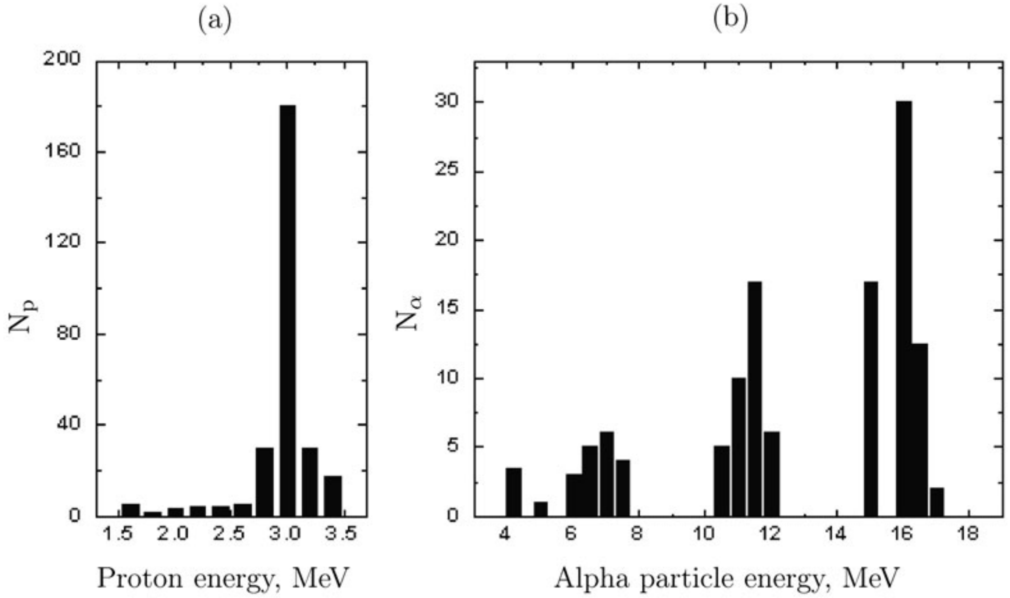

Fig. 17. The reconstructed energy spectrum of protons (a) and alpha particles (b) detected by detectors 1, 2, and 3 during Pd/PdO:D_x irradiation by electrons with 30 keV energy and 0.53 μA current density during 7020 min.

Table 1. Proton flows under the action of electron beam and X-rays on Pd/PdO:D_x and Ti/TiO_2:D_x specimens

Specimen	Detector no.	Beam	Coating thickness μm	Detectability %	3 MeV proton yield $s^{-1} \cdot cm^{-2}$ in 4π av.
Pd/PdO:D_x	1	Electrons	11 (Al)	2.6	$(1.1 \pm 0.1)\,10^{-3}$*
Pd/PdO:D_x	2	Electrons	25 (Cu)	2.6	$(1.1 \pm 0.1)\,10^{-3}$*
Pd/PdO:D_x	3	Electrons	33 (Al)	13	$(7.2 \pm 1.6)\,10^{-4}$
Ti/TiO_2:D_x	1	Electrons	11 (Al)	2.6	$(8.4 \pm 1.5)\,10^{-4}$*
Ti/TiO_2:D_x	2	Electrons	25 (Cu)	2.6	$(8.4 \pm 1.5)\,10^{-4}$*
Ti/TiO_2:D_x	8	X-rays	11 (Al)	13	$(1.5 \pm 0.3)\,10^{-2}$
Ti/TiO_2:D_x	9	X-rays	25 (Cu)	13	$(3.8 \pm 0.4)\,10^{-2}$

*Flux averaged over data from two detectors.

Under X-raying of the Ti/TiO_2:D_x, the proton yield is higher by one order of magnitude than under electron irradiation. This is primarily a result of substantially higher power of X-rays, compared to an electron beam, and probably due to the fact that X-raying acts on the bulk specimen, whereas electrons act only on its thin surface layer. Upon exposing the Pd/PdO:D_x and Ti/TiO_2:D_x to electron beam, we observe emission of primarily 3 MeV protons from both irradiated and not irradiated sides of the specimen. Therefore, the nuclear processes take place primarily in the near-surface region of the specimen, probably, at the Pd—PdO, Ti—TiO_2 interface. This can be caused by a higher deuterium concentration at the metal—dielectric interface because the radiation-stimulated deuterium diffusion in metals is much higher than in metal oxide.

Thus, the emission of 3 MeV protons stimulated by ionzing radiation of Pd/PdO:D_x, Ti/TiO_2:D_x at the room temperature unambiguously evidences that hydrogen isotopes in metals possess the unique ability to accumulate the ionizing radiation energy, as a result, the energy of deuterium atoms becomes much higher than that of the array atoms, it becomes sufficient for nuclear DD-synthesis.

2.6. Phenomenological Model of Radiation-Stimulated Diffusion and Hydrogen Release from Metals

Let us consider a model of the mechanism of nonequilibrium diffusion and release of hydrogen and its isotopes from metals stimulated by radiation, in particular, by a beam of accelerated electrons in the subthreshold energy range. Occupying equivalent positions inside metal, hydrogen forms its own subsystem in the crystal lattice, whose oscillation frequencies are outside the crystal phonon spectrum.

Upon supplying the energy by radiation, there occurs excitation of vibrational degrees of freedom in the hydrogen subsystem. The atom diffusion in the presence of the excited subsystem of light atoms can be stimulated not by the thermal oscillation energy, kT, but by the nonequilibrium oscillation energy of the internal hydrogen atmosphere, $\hbar\omega$, which is much higher than kT in the conditions of radiation stimulation. The oscillation-oscillation exchange can be effectively performed between the impurity states and the hydrogen subsystem. In these conditions, the diffusion of hydrogen and impurities becomes a nonequilibrium process stimulated by the presence of the excited hydrogen atmosphere. Contrary to the electronic subsystem, the hydrogen subsystem is capable to preserve the supplied energy for a time period sufficient for realizing the accelerated diffusion processes. Conditions of nonequilibrium radiation-stimulated release of hydrogen are determined by its concentration and the collective properties of the internal excited atmosphere. For this reason, the effects associated with nonequilibrium hydrogen release must nonlinearly grow with increasing beam current and with the injected hydrogen concentration, which is what we observe in the experiment.

3. THEORETICAL GROUNDS OF RADIATION ENERGY TRANSFER TO HYDROGEN ATOMS IN METALS

3.1. Peculiarities of the Electronic Structure of Metal–Hydrogen Systems

The described models can explain the hydrogen atom migration (a low diffusion barrier), the energy accumulation is due to radiation-excited hydrogen bonds. Nevertheless, these models cannot explain how the hydrogen atoms receive sufficient energy in order to cause nuclear processes and to let the hydrogen atoms overcome the surface barrier.

Analysis of the obtained experimental results shows that hydrogen atoms in metals can accumulate the energy of ionizing radiation (accelerated electrons and X-rays), as a result, the hydrogen subsystem transits to excited state in which the energy of hydrogen atom becomes higher by orders of magnitude than that of the array atoms. It is surprising that the hydrogen subsystem becomes excited under the action of ionizing radiation that primarily causes excitation of the electronic crystal subsystem. Meanwhile, it is known that the excited electron energy transfer to the nuclear subsystem is least probable in metals. The absence of a forbidden band and the presence of a great number of free electrons lead to rapid screening of any radiation-induced nonequilibrium charge distribution in metals, and in view of the highly efficient Auger decay, the electron excitation lifetime is substantially reduced (10^{-14}–10^{-16} s).

It is obvious that the key to understanding the mechanism of radiation energy transfer to hydrogen atoms lies in investigating the electronic structure of metal–hydrogen systems and in revealing its peculiarities that can substantially affect the process of radiation energy absorption by a crystal and also cause the radiation-stimulated nonequilibrium hydrogen migration and initiate nuclear processes. For this purpose, authors of [28, 32–35] investigated the electronic structure of the system of PdH_x, TiH_x, and pure palladium, titanium. Calculations from the first principles were performed in the context of the density functional theory by the linearized-augmented-plane-wave method [36, 37]. The exchange-correlation effects were considered using a generalized gradient approximation in the form proposed by Perdue and Wang, PW91 [38]. The chosen radii of MT spheres of hydrogen and palladium atoms were 1.9 and 0.699 at. un., respectively, thus, the hydrogen atoms could freely migrate in tetrahedral and octahedral interstitial positions of Pa face-centered cubic lattice. In the spherical harmonic expansion of the wave function inside the MT spheres, terms of up to $l = 8$ for palladium and up to $l = 4$ for hydrogen were considered. In the augmented-plane-wave expansion of the wave function, up to 120 basic functions per atom, were taken into account. At each self-consistent iteration, the Hamiltonian eigenvalues were calculated at 40 k-points of the irreducible part of Brillouin zone (IPBZ). For calculating the electronic state density N(E), there was performed linear integration of tetrahedra on a mesh of 90 k-points in the IPBZ. The function N(E) was smoothed by Gaussians with a rms width

Table 2. Lattice parameters (in a. u.) used in the calculations

	Pd	$PdH_{0.25}$	$PdH_{0.75}$	PdH
a (a.u.)	7.3512	7.5532	7.7100	7.7921

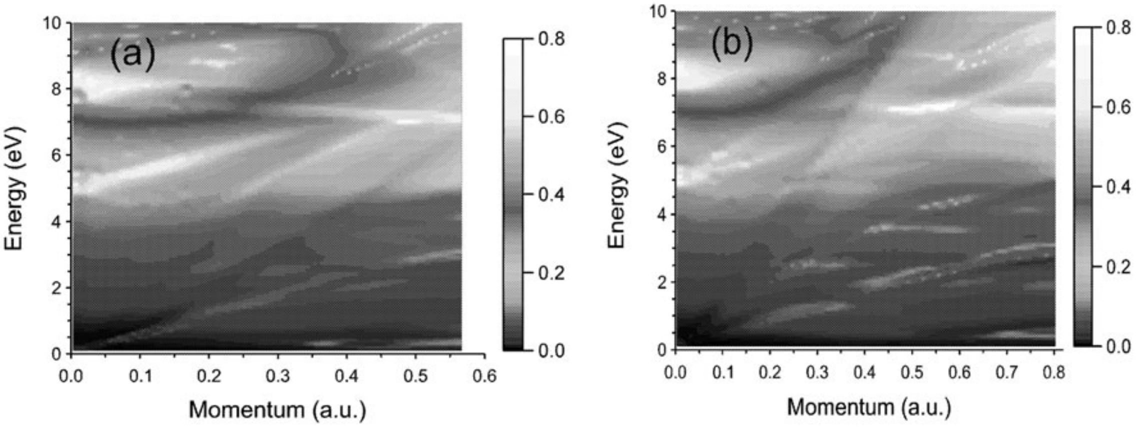

Fig. 18. The loss $\mathrm{Im}[\varepsilon^{-1}_{G=0,G'=0}(q,\omega)]$ as a function of momentum and energy for Pd along two symmetrical directions of the momentum q: (a) (100); (b) (110).

of 0.14 eV. The imaginary part of the dielectric function $\varepsilon_2(\omega)$ was calculated in an approximation of a constant matrix element on a grid of 1200 k-points in the IPBZ. The results on the calculated electronic state density for pure Pd and PdH_x solid solutions [35] show that the presence of hydrogen atoms in the Pd lattice leads to considerably changing electronic spectrum. For instance, in the PdH_x system below the valence band bottom, there appears an Hb band of bonding states resulting from hybridization of H atom s-orbitals primarily with Pd d-orbitals, which is separated by an energy gap from the complex of higher metal states. In $PdH_{0.0625}$ (low H concentration), the peak of the density of states, which corresponds to this band, is at a 7.7 eV energy, has a width of 0.5 eV, and a height of 0.07 state/eV. As the hydrogen concentration grows, the peak increases in height and becomes broader: in PdH, the peak is at a 7.7 eV energy and its height and width are 0.7 state/eV and 1.4 eV, respectively. The growing H concentration leads to filling the Pd d-band; as a result, it becomes narrower and the Fermi level of solid solution shifts upward relative to its bottom. Moreover, an additional band of Ha hybridized metal—hydrogen states appears in the PdH_x systems in the range of energies above 4.5 eV above the Fermi level (EF). It is important that for the PdH system these excited states are separated by a gap from the bound states, thus, their lifetime considerably grows, compared to the lifetime of excited states in metals. Under radiation excitation of these states in PdH, hydrogen atoms are able to leave their regular positions and diffuse in a nonequilibrium manner in the bulk specimen before the electronic subsystem relaxes to equilibrium.

3.2. Peculiarities of Collective Electronic States in Pd—H(D) *Systems*

For understanding the mechanism of the ionizing radiation energy transfer to hydrogen (deuterium) atoms that are at the specimen depth exceeding greatly the range of electrons, we studied peculiarities of collective electronic states in metal—hydrogen systems. For this purpose, authors of [39, 40] calculated the dielectric function $\varepsilon(\mathbf{r},\mathbf{r}',\omega)$, loss function $\mathrm{Im}[\varepsilon\text{-}100(q,\omega)]$, and excitation spectra for Pd and PdH_x. The calculation of dielectric matrices $\varepsilon GG'(q,\omega)$ was performed in an approximation of chaotic phases by the self-consistent norm-preserving pseudopotential method [41]. The procedure and details of the calculation are described in detail in [42]. In all the considered palladium—hydrogen systems, the hydrogen atoms were located at octahedral positions of the Pa face-centered cubic lattice. The lattice parameters used in the calculations are listed in Table 2.

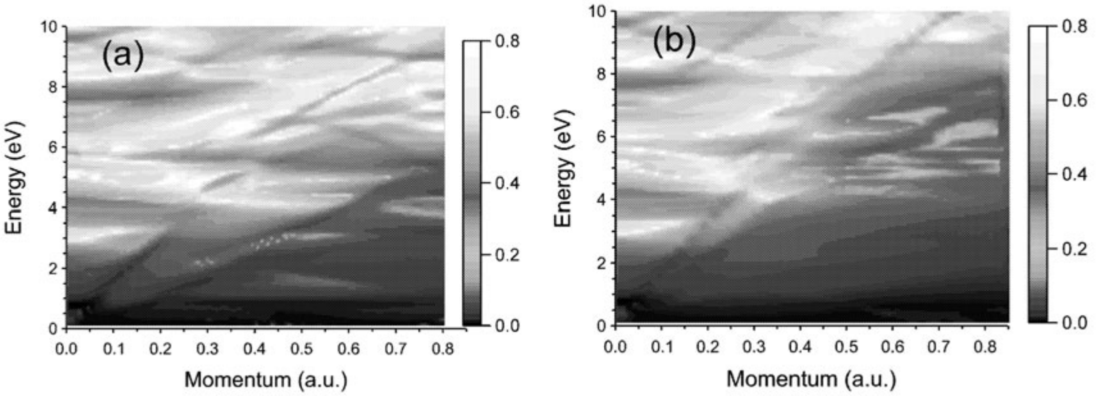

Fig. 19. The loss function $\mathrm{Im}[\varepsilon^{-1}_{G=0,G'=0}(q,\omega)]$ as a function of momentum and energy for PdH along two symmetrical directions of the momentum q: (a) (100); (b) (110).

The calculations for the loss function $\mathrm{Im}[\varepsilon^{-1}_{G=0,G'=0}(q,\omega)]$ were performed for Pd, $\mathrm{PdH}_{0.25}$, $\mathrm{PdH}_{0.75}$, and PdH along three symmetrical directions of momentum q transferred to the system under external impact (Figs. 18, 19). The figures illustrate calculations of the loss function for pure palladium and PdH along two symmetrical directions: (a) (100) and (b) (110). The dominating plasmon peak changes in the line Pd, $\mathrm{PdH}_{0.25}$, $\mathrm{PdH}_{0.75}$, and PdH from 8 eV (pure palladium) to 4.2 eV (PdH).

From the calculations (Figs. 18, 19) it follows that hydrogen adsorption modifies the palladium excitation spectrum. The most prominent effect is observed at small momenta and manifests itself in successive lowering of position of the dominating plasmon peak with the energy $\omega \approx 7.2$ eV in Pd to 4.2 eV in PdH. Excitation of the mentioned plasmons in the $\mathrm{PdH_x}$ system is the main source of losses of the external ionizing radiation after penetration to the material. On the other hand, the appeared dynamic electron density oscillations, propagating through the specimen, spend their energy primarily on excitation of collective electronic states with lower energies and a sufficiently long lifetime (of about 10^{-12}–10^{-13} s). In addition, low-energy electronic states are effective agents in energy transfer from secondary electrons, which appear in deceleration of the primary electron beam, to lattice oscillations.

CONCLUSIONS

The hydrogen and deuterium diffusion with a rate, which is noticeably higher than that of thermally equilibrium H, D diffusion in metals, can run in the presence of long-lived, on the time scale, single-phonon and electron relaxations of the oscillation-excited H, D subsystem in metals. The excited hydrogen subsystem of metals stimulates the process of diffusion not by the thermal fluctuation energy kT, but by the excess energy of nonequilibrium oscillations, $\hbar\omega_{\mathrm{H}}$, in the metal hydrogen subsystem stimulated by external ionizing radiation. In this case, the effective diffusion coefficient and rate $D^{eff}, v^{eff}\exp(-E_{act}/\hbar\omega_{\mathrm{H}})$, can substantially exceed their equilibrium values $D, v\exp(-E_{act}/kT)$.

The nonequilibrium oscillation energy depends on n_{H}, the hydrogen atom concentration in metals, and is $\hbar\omega_{\mathrm{H}} = \hbar e\sqrt{n_{\mathrm{H}}/m_p\varepsilon_0}$. Collective properties of the internal hydrogen atmosphere directly manifest themselves in the model of plasma oscillations of hydrogen isotopes in metal. The ratios of equilibrium and effective nonequilibrium diffusion coefficients are equal ($D^{eff}_{\mathrm{H}}/D > 1.4$ for H in Pd). The growth of plasma oscillation frequency with increasing hydrogen concentration explains the nonlinear effects in the dependence of the density of radiation-stimulated hydrogen isotope flux from metals on the hydrogen concentration.

The nonlinearity in the dependence of the density of hydrogen isotope flux from metals on the electron beam current is explained, in the context of the presented model, by increase in the rate of hydrogen atom release to the surface and by radiation-stimulated desorption of hydrogen molecules from the surface. The more prominent effects of electron-stimulated nonequilibrium hydrogen proton release from metals can be explained by a lower potential barrier on the way of hydrogen release from metal into vacuum. This lowering is effective under the action of electron beam because the accelerated electrons are able to neutralize H^+, D^+ ions released from the bulk to the surface, and upon colliding with H, D electron with an energy of several dozens of keV, the hydrogen atoms and molecules receive sufficient energy to release from the surface into vacuum. The photons receive a mass comparable for simple kinetic knocking-out only with an energy of $\cong$ 500 keV. In this case, the radiation penetrability of materials under study is very high such that the excitation of the hydrogen atmosphere again becomes inefficient.

Thus, the absorption of the external radiation energy and, correspondingly, the release from hydrogenated steel, niobium, and palladium depend on the microphysical parameters of the system elements, structure (presence and thickness of the metal oxide layer), oxide layer position in the structure, energy, electron beam current density, injected hydrogen concentration, and exposure time. Investigations of the electronic structure and spectra of collective electron excitations in palladium evidence their considerable changes due to hydrogen absorption. A local character of antibonding H-P states is observed. Therefore, we have concluded that the electron density oscillations in PdH_x systems corresponding to dominating plasma oscillations are localized in the vicinity of hydrogen atoms. Hydrogen considerably reduces the frequency of plasma oscillations of valence charge metal density. This evidences that the main energy of the ionizing radiation penetrating into a crystal can be absorbed due to excitation of plasmons, which, in turn, can be an effective mechanism of energy propagation through the bulk and primary localization in the vicinity of hydrogen atoms. The latter leads to nuclear reactions with proton and alpha particle release.

REFERENCES

1. Oura, K., Lifshits, V.G., Saranin, A.A., et. al., *Vvedenie v fiziku poverkhnosti* (Introduction to Surface Physics), Moscow: Nauka, 2006.
2. Wudraf, D. and Delchar, T., *Present-Day Methods for Surface Investigation*, Moscow: Mir, 1989.
3. Tyurin, Yu.I., Chernov, I.P., Krening, M., and Baumbah, H., *Radiatsionno-stimulirovannyi vykhod vodoroda iz metallov* (Radiation-Induced Hydrogen Release from Metals), Tomsk: Izd. Tomsk. Gos. Univer., 2000.
4. Tyurin, Yu.I., Semenov, A.M., and Nikitenkov, N.N., High-Vacuum Method of Measuring the Diffusion Coefficients of Light Isotopes in Metals, *Poverkh. Rentg. Sinkhr. Neitr. Issl.*, 2004, no. 5, p. 90.
5. Nikitenkov, N.N, *Izotopnyi, khimicheskii i strukturnyi analiz poverkhnosti metodami atomnoi fiziki* (Isotope, Chemical, and Structural Analysis of Surfaces by Atomic Physics Methods), Tomsk: TPU, 2002.
6. Nikitenkov, N.N. and Khoruzhii, V.D., *Issledovanie vykhoda izotopov vodoroda metodami termogazovydeleniya* (Investigation of Isotope Emission by Methods of Thermo-Gas Release), Tomsk: TPU, 2007.
7. Tyurin, Yu.I. and Chernov, I.P., *Akkumuliruyushchie svoistva vodoroda v tverdom tele* (Accumulative Hydrogen Properties in Solids), Moscow: Energoatomizdat, 2000.
8. Krachino, T.V., Kuzmin, M.V., Loginov, M.V., and Mittsev, M.A., Initial Stages of Formation of the Sm–Si(111) Interface, *FTT*, 1998, vol. 40, no. 2, pp. 371–378.
9. Denisov, E.A. and Kompaniets, T.N., The Interaction between Graphite and Atomic Hydrogen, *ZhTF*, 2001, vol. 71, iss. 2, pp. 111–116.
10. Ovchinnikov, V.V., Radiation-Dynamic Effects. The Possibilities of Formation of Unique Structural States and Properties of Condensed Media, *UFN*, 2008, vol. 178, no. 9, pp. 991–1001.
11. Prognimak, A.M., Mass-Spectrometry Investigation on the Effect of Metal-Hydride Activation of Molecular Hydrogen, *J. Hydrogen Energy*, 1995, vol. 20, no. 6, pp. 449–453.
12. Evard, E.A., Gabis, I.E., and Voyt, A.P., Study of the Kinetics of Hydrogen Sorption and Desorption from Titanium, *J. Alloys Comp.*, 2005, pp. 335–338.
13. Tyurin, Yu.I., Chernov, I.P., Cherdantsev, Yu.P., et al., Radiation-Stimulated Hydrogen Release from Metals and Alloys, *Fiz. KhOM*, 1998, no. 2, pp. 9–13.
14. Nechaev, Yu.S., Physical Complex Problems of Aging, Embrittlement, and Destruction of Metal Materials of Hydrogen Energy Production and Gas Mains, *UFN*, 2008, vol. 178, no. 7, p. 709.
15. Spivak, L.V., Synergistic Effects of Deformation Response in Thermodynamically Open Metal–Hydrogen Systems, *UFN*, 2008, vol. 178, no. 9, pp. 897–922.
16. Gapontsev, A.V. and Kondratyev, V.V., Hydrogen Diffusion in Disordered Metals and Alloys, *UFN*, 2003, vol. 173, no. 10, pp. 1108–1129.
17. Maksimov, E.G. and Pankratov, O.A., Hydrogen in Metals, *UFN*, 1975, vol. 116, no. 7, pp. 385–400.
18. Lee, Jai-Young and Lee, S.M., Hydrogen Trapping Phenomena in Metals with B.C.C. and F.C.C. Crystals Structures by the Desorption Thermal Analysis Technique, *Surf. Catal. Technol.*, 1986, vol. 28, nos. 3/4, p. 301.
19. Donovan, J.A., Accelerated Evolution of Hydrogen from Metals during Plastic Deformation, *Met. Trans.*, 1976, vol. 7a, no. 11, p. 1677.

20. Kaibyshev, O.A. and Valiev, R.Z., *Granitsy zeren i svoistva metallov* (Grain Boundaries and Metal Properties), Moscow: Metallurgiya, 1987.
21. Styrov, V.V. and Tyurin, Yu.I., *Neravnovesnye khemoeffekty na poverkhnosti trverdykh tel* (Nonequilibrium Chemoeffects on the Surface of Solids), Moscow: Energoatomizdat, 2003.
22. Fremkel, I.D. and Amfel, G., *Hydrogen in Metals*, Moscow: Mir, 1981.
23. Kozhushner, M.A. and Shub, B.R., The Probability of Formation and the Lifetime of Molecules in Vibrational Excited State in Absorption, *DAN SSSR*, 1977, vol. 237, no. 4, p. 871.
24. Ignakhina, M.A., Buravlev, Yu.M., and Gorban, E.M., Sputtering of AsB_5 Monocrystals, *Poverkh.*, 1987, no. 9, p. 141.
25. Chernov, I.P., Cherdantsev, Yu.P., and Tyurin, Yu.I., *Metody issledovaniya sistem metall—vodorod* (Methods of Investigating Metal—Hydrogen Systems), Moscow: Energoatomizdat, 2004.
26. Lipson, A.G., Chernov, I.P., Rusetskii, A.S., Tsivadze, A.Yu., Lyakhov, B.F., Cherdantsev, Yu.P., Saunin, E.I., Sakov, D.M., and Tyurin, Yu.I., Desorption of Hot Deuterium Atoms from the $Pd/PdO:D_x$ Heterostructure under Excitation of Its Hydrogen Subsystem, *Dokl. Phys.*, 2009, vol. 54, no. 4, pp. 182—186.
27. Chernov, I.P., Rusetskii, A.S., Krasnov, D.N., Larionov, V.V., Tyurin, Yu.I., and Cherdantsev, Yu.P., Nuclear Reactions in Pd/PdO:D and Ti/TiO:D Systems Excited by Ionizing Radiation, *ZhETF*, 2011, vol. 139, iss. 6, pp. 1088—1098.
28. Chernov, I.P., Cherdantsev, Yu.P., Lider, A.M., Garanin, G.V., and Surkov, A.A., Hydrogen Behavior in Stainless Steel during Irradiation, *Poverkh. Rentg. Sinkhr. Neitr. Issl.*, 2007, no. 7, pp. 10—18.
29. Lipson, A.G., Lyakhov, B.F., Roussetski, A.S., et al., *Fus. Technol.*, 2000, vol. 38, p. 238.
30. Styrov, V.V., Tyurin, Yu.I., and Grankin, V.P., Self-Oscillation Reaction of Atom Recombination, *ZhETF*, 2002, vol. 121, no. 2, pp. 274—285.
31. Popov, V.V., Basteev, A.V., Solovey, V.V., and Prognimak, A.M., The Effect of Metal-Hydride Activation of Hydrogen and Investigation of Its Influence on the Characteristics of Gas-Discharge Hydrogen-Using Energy Conversion Devices, *Int. J. Hydr. Energy*, 1996, vol. 21, no. 4, pp. 259—265.
32. Koroteev, Yu.M., Gimranova, O.V., and Chernov, I.P., Dielectric Response Function of PdH_x System, *Izv. Tomsk. Polytech. Univ.*, 2006, vol. 309, no. 4, pp. 56—60.
33. Chernov, I.P., Koroteev, Yu.M., Gimranova, O.V., and Garanin, G.V., The Mechanism of Nonequilibrium Hydrogen Migration in Metals under Ionizing Irradiation, *Alt. Energ. Ekol.*, 2006, no. 8(40), pp. 75—78.
34. Chernov, I.P., Koroteev, Yu.M., Gimranova, O.V., and Tyurin, Yu.I., The Role of Hydrogen in Ionizing Radiation Energy Absorption by Metal—Hydrogen System, *Poverkh. Rentg. Sinkhr. Neitr. Issl.*, 2007, no. 4, pp. 16—21.
35. Chernov, I.P., Koroteev, Yu.M., Silkin, V.M., and Tyurin Yu.I., Evolution of the Electron Structure and Excitation Spectrum in Palladium as a Result of Hydrogen Absorption, *Dokl. Phys.*, 2008, vol. 53, no. 6, pp. 318—322.
36. Wimmer, E., Krakauer, H., Weinrt, M., and Freeman, A.J., Full-Potential Self-Consistent Linearized-Augmented-Plane-Wave Method for Calculating the Electronic Structure of Molecules and Surfaces: O_2 Molecule, *Phys. Rev. B*, 1981, vol. 24, pp. 864—875.
37. Weinert, M., Wimmer, E., and Freeman, A.J., Total-Energy All-Electron Density Functional Method for Bulk Solids and Surfaces, *Phys. Rev. B*, 1982, vol. 26, pp. 4571—4578.
38. Wang, Y. and Perdew, J.P., Correlation Hole of the Spin-Polarized Electron Gas, with Exact Small-Wave-Vector and High-Density Scaling, *Phys. Rev. B*, 1991, vol. 44, pp. 13298—13307.
39. Silkin, V.M., Chernov, I.P., Echenique, P.M., Koroteev, Yu.M., and Chulkov, E.V., Influence of Hydrogen Absorption on Low-Energy Electronic Collective Excitations in Palladium, *Phys. Rev. B*, 2007, vol. 76, pp. 245105—245109.
40. Silkin, V.M., Chernov, I.P., Koroteev, Yu.M., and Chulkov, E.V., Low-Energy Collective Electronic Excitations in Pd Metal, *Phys. Rev.*, 2009, vol. B 80, pp. 245114—245121.
41. Nechaev, A., Zhukov, V.P., and Chulkov, E.V., Ab initio GW Calculations of the Time and Length of Spin Relaxation of Excited Electrons in Metals with Inclusion of the Spin-Orbit Coupling, *Phys. Sol. State*, 2007, vol. 49, no. 4, p. 1811.
42. Troullier, N. and Martins, J.L., Efficient Pseudopotentials for Plane-Wave Calculations, *Phys. Rev. B*, 1991, vol. 43, no. 3, pp. 1993—2006.